JACC: CARDIOVASCULAR IMAGING VOL. 7, NO. 4, 2014

ISSN 1936-878X/$36.00
PUBLISHED BY ELSEVIER INC. http://dx.doi.org/10.1016/j.jcmg.2014.01.001

Diagnostic Value of PET-Measured Longitudinal Flow Gradient for the Identification of Coronary Artery Disease

Ines Valenta, MD,* Alessandra Quercioli, MD,† Thomas H. Schindler, MD*

Baltimore, Maryland; and Geneva, Switzerland

OBJECTIVES The purpose of this study was to evaluate the diagnostic value of a positron emission tomography (PET)/computed tomography (CT)–determined longitudinal decrease in myocardial blood flow (MBF) gradient during hyperemia and myocardial flow reserve (MFR) for the identification of epicardial stenosis ≥50%.

BACKGROUND Although PET-determined reductions in MFR are increasingly applied to identify epicardial lesions in coronary artery disease (CAD), it may be seen as a suboptimal approach due to the nonspecific origin of decreases in MFR.

METHODS In 24 patients with suspected or known CAD, MBF was measured with ^{13}N-ammonia and PET/CT in ml/g/min at rest, during dipyridamole stimulation, and the corresponding MFR was calculated. MBF was also determined in the mid and mid-distal myocardium of the left ventricle (LV). A decrease in MBF from mid to mid-distal LV myocardium was defined as longitudinal MBF gradient. MBF parameters were determined in the myocardial region with stress-induced perfusion defect and with stenosis ≥50% (territory 1), without defect but with stenosis ≥50% (territory 2), or without stenosis ≥50% (territory 3).

RESULTS In territories 1 and 2 with focal stenosis ≥50%, the severity of epicardial artery stenosis correlated with the Δlongitudinal MBF gradient (stress-rest) ($r = 0.52$; $p < 0.0001$), while this association was less pronounced for corresponding MFR ($r = -0.40$; $p < 0.003$). On a vessel-based analysis, the sensitivity and specificity of the Δlongitudinal MBF gradient in the identification of epicardial lesions was higher than those for MFR (88% vs. 71%, $p \leq 0.044$; and 81% vs. 63%, $p = 0.134$, respectively). Combining both parameters resulted in an optimal sensitivity of 100% and intermediate specificity of 75%. The diagnostic accuracy was highest for the combined analysis than for the Δlongitudinal MBF gradient or MFR alone (94% vs. 86%, $p \leq 0.003$; and 94% vs. 70%, $p \leq 0.0002$).

CONCLUSIONS The combined evaluation of a Δlongitudinal MBF gradient and MFR may evolve as a new promising analytic approach to further optimize the identification of CAD lesions. (J Am Coll Cardiol Img 2014;7:387–96) © 2014 by the American College of Cardiology Foundation

From the *Division of Nuclear Medicine, Department of Radiology, and Division of Cardiology, Department of Medicine, Johns Hopkins University, Baltimore, Maryland; and the †Department of Specialties in Medicine, University Hospitals of Geneva, Geneva, Switzerland. This study was supported by a departmental fund from Johns Hopkins University, with contributions of the Clinical Research Center, University Hospital, and Faculty of Medicine, Geneva; the Louis-Jeantet Foundation; and the Swiss Heart Foundation. Dr. Schindler has received research grant no. 3200B0-122237 from the Swiss National Science Foundation; and has received support from the Gustave and Simone Prévot fund. All other authors have reported that they have no relationships relevant to the contents of this paper to disclose.

Manuscript received October 18, 2013; revised manuscript received January 5, 2014, accepted January 7, 2014.

JACC: CARDIOVASCULAR IMAGING, VOL. 7, NO. 4, 2014
APRIL 2014:387–96

Assessment of left ventricular (LV) myocardial blood flow (MBF) at rest, during pharmacologically stimulated hyperemia, and the resulting myocardial flow reserve (MFR) with positron emission tomography (PET) or PET/computed tomography (CT) is increasingly applied to assess the flow-limiting effects of single lesions in multivessel coronary artery disease (CAD) (1–4). Such noninvasively-obtained information on hyperemic MBF and MFR has also been demonstrated to carry important prognostic information in patients with and without clinically-manifest CAD (5–7). Reductions in MFR in CAD patients, however, may be interpreted not only as a consequence of flow-limiting effects of epicardial stenosis, if present, but also in the context of microvascular dysfunction (3,7). Due to the relatively low specificity of reduced MFR (7,8), a clear identification of flow-limiting effects of epicardial lesions in the individual CAD patient sometimes may remain uncertain. In this direction, PET flow measurements of an abnormal decrease in MBF from the base to the apex of the LV during hyperemic flows, a so-called flow gradient, has been suggested to provide more detailed information on structural and functional alterations of epicardial artery in cardiovascular risk individuals (9–12). This proximal-to-distal flow gradient has been attributed to fluid dynamic consequences of CAD-induced diffuse luminal narrowing or to functional alterations of the epicardial coronary conduit vessels (9,10,13). As the longitudinal MBF gradient is assumed to be related predominantly to increases in epicardial resistance during hyperemic flows (12,13), it may provide more specific information on flow-limiting effects of epicardial stenosis than the conventional interpretation of MFR alone. According to this, we aimed to determine the diagnostic value of a PET/CT-determined longitudinal decrease in MBF (MBF gradient) during hyperemia and MFR for the identification of epicardial stenosis ≥50% in CAD patients.

ABBREVIATIONS AND ACRONYMS

CAD = coronary artery disease
CT = computed tomography
CVR = coronary vascular resistance
LAD = left anterior descending
LCx = left circumflex
LV = left ventricular
MBF = myocardial blood flow
MFR = myocardial flow reserve
PET = positron emission tomography
RCA = right coronary artery
ROC = receiver-operating characteristic
RPP = rate-pressure product
SDS = summed difference score
SSS = summed stress score

METHODS

Patient population. The study population comprised 24 patients (18 men, 6 women; mean age 67 ± 10 years) with stress-induced regional myocardial perfusion defects on ^{13}N-ammonia PET/CT images. Within 20 days of PET perfusion imaging, these patients underwent invasive coronary angiography (Table 1). Quantitative coronary angiography was performed to assess the severity of epicardial lesions identified during invasive coronary angiography. Patients were considered for study purposes, if coronary artery lesions of ≥50% diameter stenosis were located in the proximal part of the left anterior descending (LAD) (segments 12 to 13), left circumflex (LCx) (segments 18 to 19), and right coronary artery (RCA) (segments 1 to 3) according to the American College of Cardiology/American Heart Association guidelines (14). All CAD patients had normal wall motion on angiographic evaluation. In addition, 34 healthy individuals without known cardiovascular risk factors and normal stress-rest ^{13}N-ammonia PET/CT perfusion imaging served as a control group (Table 1). Cardiovascular risk factors included the presence of arterial hypertension, smoking, type 2 diabetes mellitus, hypercholesterolemia, or family history of CAD. Patients with evidence of left ventricular hypertrophy on echocardiography were excluded from study analysis. Vasoactive medications such as calcium-channel blockers, angiotensin-converting enzyme inhibitors, statins, as well as beta-blockers, and diuretics were discontinued at least 24 h before PET flow study. All study participants refrained from caffeine-containing beverages for ≥24 h and from smoking for ≥12 h prior to the PET study. The study was approved by the University Hospitals of Geneva Institutional Review Board (No. 07-184), and each participant signed the approved informed consent form.

PET/CT flow investigations. Myocardial perfusion and MBF, measured in ml/min/g, were assessed with ^{13}N-ammonia PET/CT, serial PET image acquisition (64-slice Biograph, HiRez TruePoint PET-CT scanner, Siemens Medical Solutions, Erlangen, Germany), and a 2-compartment tracer kinetic model, as described in detail previously (12). Pharmacologic vasodilation to stimulate hyperemic MBF increases was performed with standard infusion of dipyridamole (140 μg/kg/min). Myocardial perfusion at rest and during pharmacologic vasodilation was analyzed visually on reoriented short- and long-axis myocardial slices and semiquantitatively on the corresponding polar map from the last static 18-min transaxial PET image. For the semiquantitative analysis of the PET perfusion images, a 17-segment model and a 5-point grading system by 2 expert observers were applied (12). Summed stress score (SSS), summed rest score, and summed difference score (SDS) were calculated. An SSS <4 was considered normal, 4 to 8 mildly abnormal, 9 to 13 moderately abnormal, and >13 severely

abnormal perfusion defect. Further, a SDS ≥2 identified a reversible perfusion defect, whereas <2 was considered as normal. The extent of regional reversible perfusion defects on ^{13}N-ammonia PET/CT images was graded according to the SDS value. Accordingly, an SDS of 2 to 4, >5 to 8, and >8 defined mild, moderate, and severe reversible perfusion defects, respectively. Regional MBFs of the 3 main myocardial territories subtended to the LAD, LCx, and RCA were averaged on a polar map, and the resulting mean MBF of the LV was defined as global MBF. Subsequently, longitudinal MBFs in the mid and mid-distal myocardial segment of the LV corresponding to the vascular territories of the LAD (segments: 7 to 8 and 13 to 14), LCx (segments: 11 to 12 and 16), and RCA (segments: 9 to 10 and 15) were determined. Basal segments (LAD: 1 to 2, LCx: 5 to 6, and RCA: 3 to 4) and the apical segment (LAD: 17), however, were not included for this analysis due to a possible count variability induced by the membranous septum, by a certain variability in locating the last apical slice, and by partial volume errors resulting from object size at the apex (9). Heart rate, blood pressure, and a 12-lead electrocardiogram were recorded continuously during each MBF measurement. From the average of heart rate and systolic blood pressure during the first 2 min of each image acquisition, the rate-pressure product (RPP) (heart rate × systolic blood pressure) was derived as an index of myocardial workload. A decrease in MBF from mid to mid-distal LV myocardium (ml/g/min) was defined as longitudinal, base-to-apex MBF gradient. Alterations in the longitudinal, base-to-apex MBF gradient from rest to dipyridamole-stimulated hyperemia were defined as rest-to-stress change in longitudinal, base-to-apex MBF gradient (Δlongitudinal MBF gradient = longitudinal MBF gradient during hyperemia − longitudinal MBF gradient at rest). To account for interindividual variations in coronary driving pressure, an index of coronary vascular resistance (CVR) was determined as the ratio of mean arterial blood pressure (mm Hg) to MBF (ml/g/min). As resting MBF is dependent on the myocardial workload, it was normalized to the RPP (averaged during the first 2 min of image acquisition; MBF/RPP × 10,000). This again served to calculate the corrected MFR: (hyperemic MBF during dipyridamole)/(NMBF at rest).

Statistics. Because continuous variables are not always normally distributed, they are presented as median and interquartile range (IQR) (25th to 75th percentile: quartile 1, quartile 3). For comparison of differences, we used the Mann-Whitney U test for independent samples (SPSS statistics 22.0, IBM, Armonk, New York). A comparison of flow parameters among different myocardial territories was performed by Kruskal-Wallis 1-way analysis of variance. Pearson correlation coefficients (r), assuming a linear regression and the standard error of the estimate (SEE), were calculated to investigate the associations between various flow parameters and epicardial stenosis diameter, respectively. Using the Fisher r-to-z transformation, the significance of differences between related correlations was determined. Receiver-operating characteristic (ROC) curve with the Youden index (J) was used to define the best flow threshold for the Δlongitudinal MBF gradient and MFR in the detection of ≥50% diameter stenosis. The McNemar test was used to compare the diagnostic accuracy, sensitivity, and specificity of flow parameters in the detection of CAD. All test procedures were 2-sided with a p value ≤0.05, indicating statistical significance.

Table 1. Clinical Characteristics of the Study Population

	Control Individuals (n = 34)	CAD Patients (n = 24)	p Values
Age, yrs	39 (32, 45)	56 (52, 59)	0.0001
BMI, kg/m^2	22 (21, 26)	30 (27, 34)	0.0001
Risk factors			
Hypertension	0 (0)	11 (45)	—
Smoking	0 (0)	9 (37)	—
Hypercholesterolemia	0 (0)	13 (54)	—
Obesity	0 (0)	5 (21)	—
Family history of CAD	0 (0)	4 (17)	—
Diabetes mellitus	0 (0)	7 (29)	—
Fasting plasma concentrations, mg/dl			
Cholesterol	206 (167, 230)	227 (209, 240)	0.014
LDL	125 (102, 146)	140 (123, 163)	0.027
HDL	49 (36, 71)	39 (33, 48)	0.030
TG	74 (54, 168)	98 (67, 178)	0.198
Glucose	90 (84, 102)	113 (102, 123)	0.001
hsCRP	1.0 (0.9, 2.0)	8.5 (0.8, 17.7)	0.013

Values are median (Q1, Q3) or n (%). p values versus control individuals (Mann-Whitney U test for independent samples).
BMI = body mass index; CAD = coronary artery disease; HDL = high-density lipoprotein; hsCRP = high-sensitivity C-reactive protein; LDL = low-density lipoprotein; TG = triglycerides.

RESULTS

Clinical characteristics. Table 1 denotes the characteristics of the study population. All patients had a history of angina pectoris: 20 with suspicion for

Table 2. Myocardial Flow Parameters and Hemodynamics in Control Individuals and CAD Patients During PET/CT

	Control Individuals	CAD Patients	p Value
Flow parameters			
Global MBF			
Rest	0.70 (0.65, 0.72)	0.89 (0.76, 1.19)	0.0001
DP	2.16 (1.85, 2.57)	1.29 (1.02, 1.52)	0.0001
Global NMBF—rest	0.95 (0.85, 1.14)	1.00 (0.93, 1.08)	0.528
Global MFR	3.17 (2.81, 3.75)	1.32 (1.17, 1.73)	0.0001
Global corrected MFR	3.51 (2.63, 4.02)	1.27 (1.05, 1.57)	0.0001
Global CVR			
Rest	119 (105, 134)	98 (88, 125)	0.010
DP	37 (29, 42)	66 (56, 74)	0.0001
Global ΔCVR	−82 (−100, −68)	−28 (−56, −18)	0.0001
MBF gradient			
Rest	−0.04 (−0.08, −0.04)	−0.09 (−0.14, −0.01)	0.339
DP	−0.09 (−0.12, −0.07)	−0.28 (−0.34, −0.20)	0.0001
ΔMBF gradient	−0.04 (−0.07, −0.01)	−0.16 (−0.28, −0.10)	0.0001
CVR gradient			
Rest	9.35 (4.91, 12.74)	5.84 (0.19, 15.28)	0.324
DP	1.50 (1.02, 2.13)	15.01 (8.35, 20.03)	0.0001
ΔCVR gradient	−7.45 (−11.54, −3.49)	6.09 (−0.31, 17.04)	0.0001
Hemodynamics			
Heart rate, beats/min			
Rest	63 (59, 70)	71 (63, 79)	0.002
DP	90 (78, 94)	81 (71, 87)	0.009
SBP, mm Hg			
Rest	115 (103, 120)	128 (115, 139)	0.001
DP	110 (105, 118)	119 (113, 132)	0.014
RPP			
Rest	7,192 (6,600, 7,705)	8,579 (7,873, 10,110)	0.0001
DP	9,375 (9,549, 10,620)	9,252 (8,451, 10,339)	0.765

Values are median (Q1, Q3). p values versus control individuals (Mann-Whitney *U* test for independent samples). Corrected MFR = ratio of MBF-DP to NMBF at rest. RPP = HR × SBP.
CT = computed tomgraphy; CVR = coronary vascular resistance (mm Hg/ml/g/min); DP = dipyridamole; HR = heart rate; MBF = myocardial blood flow (ml/g/min); MFR = myocardial flow reserve; NMBF = normalized myocardial blood flow (ml/g/min); PET = positron emission tomography; RPP = rate-pressure product; SBP = systolic blood pressure; other abbreviations as in Table 1.

CAD and 4 with known CAD. When a significant epicardial coronary artery lesion during coronary angiography was defined as ≥50% diameter stenosis, 9 patients had 1-vessel disease, 13 had 2-vessel disease, and 7 had 3-vessel disease.

Stress-induced myocardial perfusion defects. In 24 patients with suspected and known CAD, ^{13}N-ammonia PET/CT with stress and rest images identified 29 regional reversible perfusion defects (abnormal SSS ≥4 and SDS ≥2). The mean summed rest score, SSS, and SDS were 1.6 ± 0.9, 7.7 ± 2.3, and 6.1 ± 2.0, respectively. All reversible perfusion defects on ^{13}N-ammonia PET/CT were subtended to epicardial lesions ≥50% diameter stenosis as evidenced by invasive coronary angiography. Five patients had 2 stress-induced perfusion defects with regional decreases in ^{13}N-ammonia concentrations ≥2.5 SDs below the mean in different myocardial territories on standard polar map evaluation. On a vessel-based analysis, there were 21% (6 of 29) mild, 62% (18 of 29) moderate, and 17% (5 of 29) severe reversible perfusion defects.

Hemodynamics, global and regional flow parameters. Resting heart rate, systolic blood pressure, and corresponding RPP were observed to be higher in CAD patients than in control individuals (Table 2). Because MBF commonly follows the RPP during resting conditions, CAD patients had higher resting MBFs than control individuals. During dipyridamole-stimulated hyperemia, heart rate increased significantly from rest in both groups, and was higher in control individuals. Conversely, there was a mild and nonsignificant decrease in systolic blood pressure during dipyridamole-stimulation in control individuals, whereas it was significant in the CAD group. Although the RPP during pharmacologic vasodilation was comparable among these 2 groups, global hyperemic MBF and MFR were significantly higher in control individuals than in CAD patients. When the global hyperemic MBF was related to the mean arterial blood pressure in order to compensate for possible interindividual variations in coronary driving pressure, the resulting estimates of global CVR (mean arterial blood pressure/MBF) widely mirrored the MBF values at rest and during pharmacologic vasodilation for each group studied (Table 2). Thus, differences in coronary driving pressure during pharmacologic vasodilation do not account for alterations in hyperemic MBF responses.

Longitudinal, base-to-apex MBF gradient. Resting regional MBF was significantly lower in the mid-distal than in the mid-LV myocardium in both groups of control individuals and CAD patients (median 0.62 ml/g/min [IQR: 0.57, 0.69 ml/g/min] vs. 0.68 ml/g/min [IQR: 0.61, 0.72 ml/g/min] and 0.89 ml/g/min [IQR: 0.78, 0.96 ml/g/min] vs. 1.03 ml/g/min [IQR: 0.79, 1.14 ml/g/min], respectively; $p < 0.0001$). This resulted in small and comparable longitudinal MBF gradients at rest between the 2 groups (Table 2). During hyperemic MBFs, the decrease in longitudinal flow from the base to apex direction was more pronounced in CAD than in control individuals (median 1.33 ml/g/min [IQR: 1.34, 1.63 ml/g/min]

to 1.12 ml/g/min [IQR: 0.92, 1.42 ml/g/min] and 2.22 ml/g/min [IQR: 1.92, 2.64 ml/g/min] to 2.09 ml/g/min [IQR: 1.85, 2.50 ml/g/min]), which resulted in a significantly higher longitudinal MBF gradient during pharmacologic vasodilation and Δlongitudinal MBF gradient in CAD patients when compared with control individuals (Table 2).

When looking at resting longitudinal flows in the territory with the stress-induced perfusion defect (T1) and the territory without stress-induced perfusion defect but with stenosis ≥50% (T2) or without stenosis ≥50% (T3) (Table 3), regional MBF was also significantly lower in the mid-distal than in the mid-LV myocardium ($p < 0.0001$, respectively). The resting longitudinal MBF gradient, however, was not significantly different among myocardial territories T1 to T3 (Table 3). When regional hyperemic MBFs were evaluated in T1 to T3 in these CAD patients, they were significantly lower in the mid-distal than in the mid-LV myocardium. The corresponding longitudinal MBF gradient during pharmacologic vasodilation and the change in longitudinal MBF gradient from rest to hyperemia defined as Δlongitudinal MBF gradient (longitudinal MBF gradient during hyperemia − longitudinal MBF gradient at rest) progressively increased from T1 to T2 and T3, respectively (Table 3). Although the longitudinal MBF gradient during pharmacologic vasodilation was significantly higher in T3 than in T2, it did not reach statistical significance for the Δlongitudinal MBF gradient. In addition, the longitudinal MBF gradient during pharmacologic vasodilation and Δlongitudinal MBF gradient in T3 were significantly more pronounced than that observed in control individuals ($p = 0.0001$ and $p = 0.001$)

Table 3. Myocardial Flow Parameters in Territories With and Without Stress-Induced PD During PET/CT

	Territory With PD (T1)	Territory Without PD and With Stenosis ≥50% (T2)	p Values (T2 vs. T1)	Territory Without Both PD and Stenosis ≥50% (T3)	p Values (T3 vs. T1)	p Values (T3 vs. T2)
Regional flow parameters						
MBF—rest	0.83 (0.68, 1.13)	1.03 (0.78, 1.21)	0.099	0.85 (0.74, 1.03)	0.713	0.223
NMBF—rest	0.93 (0.83, 1.09)	1.07 (0.95, 1.24)	0.025	0.99 (0.87, 1.10)	0.505	0.251
MBF—DP	1.18 (0.85, 1.31)	1.32 (1.15, 1.60)	0.004	1.32 (1.03, 1.68)	0.055	0.753
MFR	1.19 (1.0, 1.64)	1.28 (1.16, 1.73)	0.192	1.36 (1.25, 1.81)	0.026	0.436
Corrected MFR	1.24 (0.93, 1.36)	1.22 (1.04, 1.68)	0.411	1.23 (1.08, 1.54)	0.446	0.949
Longitudinal flow parameters						
MBF at rest						
Mid-LV segment	0.95 (0.64, 1.15)	1.05 (0.82, 1.17)	0.279	0.98 (0.79, 1.13)	0.491	0.466
Mid-distal segment	0.89 (0.69, 1.01)	0.93 (0.81, 1.07)	0.323	0.86 (0.74, 1.01)	0.887	0.204
Gradient	−0.02 (−0.14, 0.02)	−0.07 (−0.15, 0.0)	0.504	−0.09 (−0.17, −0.07)	0.144	0.159
MBF during DP						
Mid-LV segment	1.23 (1.04, 1.39)	1.46 (1.15, 1.71)	0.020	1.56 (1.28, 2.0)	0.009	0.379
Mid-distal segment	1.09 (0.85, 1.22)	1.14 (0.88, 1.39)	0.441	1.28 (1.03, 1.56)	0.107	0.451
Gradient	−0.16 (−0.19, −0.11)	−0.31 (−0.39, −0.23)	0.0001	−0.45 (−0.56, −0.33)	0.001	0.037
ΔGradient	−0.10 (−0.14, −0.03)	−0.21 (−0.35, −0.10)	0.001	−0.39 (−0.45, −0.14)	0.002	0.247
CVR at rest						
Mid-LV segment	100 (84, 129)	93 (74, 110)	0.110	104 (82, 111)	0.449	0.687
Mid-distal segment	117 (87, 127)	96 (82, 111)	0.139	103 (92, 120)	0.641	0.509
Gradient	4.12 (−2.03, 13.6)	6.50 (0.0, 12.7)	0.610	7.58 (3.34, 9.91)	0.440	0.834
CVR during DP						
Mid-LV segment	68 (59, 78)	57 (49, 68)	0.008	63 (48, 67)	0.140	0.680
Mid-distal segment	78 (64, 92)	72 (62, 85)	0.574	77 (58, 104)	0.924	0.704
Gradient	10.84 (6.14, 13.47)	15.50 (11.39, 23.81)	0.009	23.60 (12.06, 36.90)	0.027	0.465
ΔCVR gradient	3.24 (−1.34, 11.67)	11.18 (3.59, 19.27)	0.053	17.23 (3.38, 25.29)	0.052	0.568

Values are median (Q1, Q3). Territory 1 (T1), stress-induced perfusion defect (PD). Territory 2 (T2), no stress-induced PD and stenosis ≥50%. Territory 3 (T3), no stress-induced PD and without stenosis ≥50%. p values according to Mann-Whitney *U* test for independent samples.
Abbreviations as in Table 2.

(Tables 2 and 3). As regards the post-stenotic Δlongitudinal MBF gradient in T1 and T2, it did not differ significantly among the LAD (n = 19), LCx (n = 17), and RCA territories (n = 20) (median −0.10 ml/g/min [IQR: −0.19, −0.09 ml/g/min] vs. −0.16 [IQR: −0.29, −0.01 ml/g/min] vs. −0.14 [IQR: −0.21, −0.07 ml/g/min]; p = 0.960 by analysis of variance).

Correlations between regional MFR, Δlongitudinal MBF gradient, and epicardial stenosis. To investigate a possible association between hyperemic flow parameters and epicardial stenosis, the quantitatively-measured severity of epicardial stenosis was related to the corresponding regional post-stenotic Δlongitudinal MBF gradient and MFR, respectively. For the entire CAD study group with focal lesions ≥50% (T1 to T2), the severity of epicardial artery stenosis closely correlated with the Δlongitudinal MBF gradient (Fig. 1A). As the Δlongitudinal MBF gradient may have been affected by interindividual differences in coronary driving pressure, the relationship between the Δlongitudinal CVR and the severity of epicardial artery stenosis was evaluated. As seen in Fig. 1B, there was a less pronounced but still significant association between Δlongitudinal CVR and the stenosis severity. In regard to the regional MFR, it correlated inversely and significantly with stenosis severity (Fig. 1C), although this association was less prominent for the corrected MFR (Fig. 1D). Although the correlation coefficient of 0.52 between the Δlongitudinal MBF gradient and epicardial artery stenosis (Fig. 1A) is stronger than that between regional MFR and epicardial artery stenosis of 0.40 (Fig. 1C), the difference between these correlation coefficients did not reach statistical significance (p = 0.198).

Furthermore, we analyzed the relationship between hyperemic MBF increases and post-stenotic Δlongitudinal MBF gradient in T1 and T2 (Fig. 2). As it can be observed, hyperemic MBFs inversely correlated with the post-stenotic Δlongitudinal

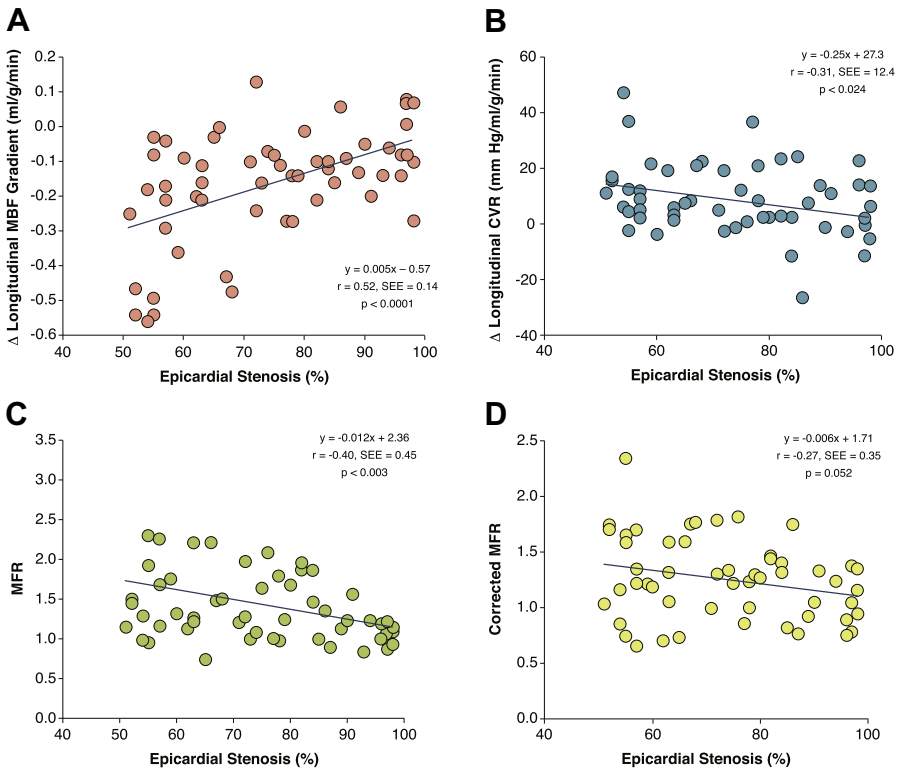

Figure 1. Relationship Among ΔLongitudinal MBF Gradient, ΔLongitudinal CVR, MFR, Corrected MFR, and Severity of Epicardial Stenosis

(A) Correlation between Δlongitudinal myocardial blood flow (MBF) gradient and percent diameter stenosis (negative values on the y-axis indicate an increase in Δlongitudinal MBF gradient). **(B)** Inverse correlation between Δlongitudinal coronary vascular resistance (CVR) and percent diameter stenosis (positive values on the y-axis indicate an increase in Δlongitudinal CVR). **(C)** Correlation between myocardial flow reserve (MFR), **(D)** corrected MFR, and percent diameter stenosis. SEE = standard error of the estimate.

MBF gradient ($r = -0.29$, SEE = 0.16, $p < 0.02$), emphasizing the flow velocity as an important determinant for the extent of Δlongitudinal MBF gradient. When performing a 4-quadrant analysis, it can be appreciated that the inverse correlation is mostly related to the upper-left and lower-right quadrants. It also appears that the higher the hyperemic MBF value, the less is the variability for the post-stenotic Δlongitudinal MBF gradient (upper-left quadrant). Conversely, the relationship between hyperemic MBF and post-stenotic Δlongitudinal MBF gradient may not exist when regarding the lower flow range of the post-stenotic Δlongitudinal MBF gradient (lower- and upper-right quadrant), suggesting an uncoupling of the post-stenotic Δlongitudinal MBF gradient from hyperemic MBFs.

Diagnostic accuracy of regional MFR and Δlongitudinal MBF gradient in the detection of CAD lesions. The ROC for the detection of epicardial stenosis ≥50% by regional MFR and Δlongitudinal MBF gradient yielded an optimal cutoff point of ≤1.40 and ≤0.25 ml/g/min, respectively. When applying this ROC-defined threshold on a per-vessel basis, the sensitivity, specificity, NPV, PPV, and diagnostic accuracy of the Δlongitudinal MBF gradient, MFR, and the combined analysis of both parameters for the detection of epicardial stenosis are given in Table 4. The sensitivity of the Δlongitudinal MBF gradient to identify epicardial lesions was significantly higher than for the regional MFR (88% vs. 71%; $p \leq 0.044$) (Fig. 3), and combining both parameters resulted in an optimal sensitivity of 100%. As regards the specificity, it was nonsignificantly higher for the Δlongitudinal MBF gradient than for the regional MFR (81% vs. 63%; $p = 0.134$). Applying both flow parameters resulted in an intermediate specificity of 75% that was lower than for the Δlongitudinal MBF gradient (81%) and higher than for the MFR (63%), but nonsignificantly ($p = 1.00$). The diagnostic accuracy of the Δlongitudinal MBF gradient for evaluation of epicardial stenosis was nonsignificantly higher compared with the MFR (86% vs. 70%; $p = 0.307$). The combined analysis of both parameters, however, yielded the highest diagnostic accuracy that was significantly higher than those for the Δlongitudinal MBF gradient and for MFR alone (94% vs. 86%, $p \leq 0.003$; and 94% vs. 70%, $p \leq 0.0002$).

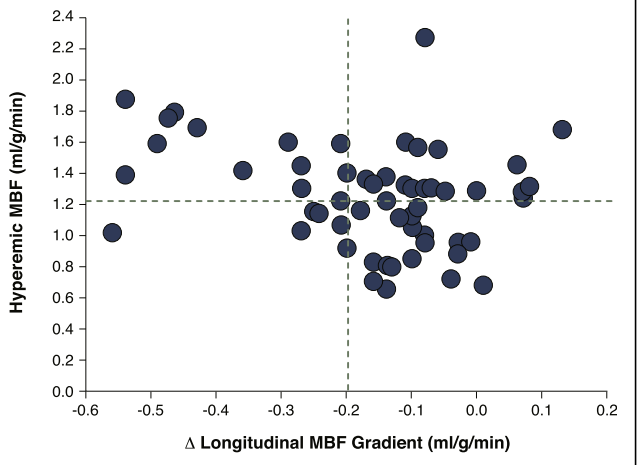

Figure 2. Relationship Between Hyperemic MBFs and ΔLongitudinal MBF Gradient in the Post-Stenotic Myocardial Territory

Correlation between hyperemic myocardial blood flows (MBFs) and corresponding post-stenotic Δlongitudinal MBF gradient in a 4-quadrant display (negative values on the x-axis indicate an increase in Δlongitudinal MBF gradient).

DISCUSSION

The present study is unique in that it demonstrates a modest but significant association between focal epicardial stenosis severity and a post-stenotic Δlongitudinal MBF gradient from the mid to mid-distal LV myocardium. In CAD patients, therefore, increases in severity of epicardial lesions were paralleled by a progressive decrease in the magnitude of a post-stenotic Δlongitudinal MBF gradient. As intracoronary resistance relates inversely not only to the vessel diameter, but also to the velocity of the blood flow according to the Hagen-Poiseuille law (13,15); advanced epicardial artery lesions may have offset the post-stenotic longitudinal MBF gradient during hyperemic flows due to a stenosis-induced decrease in hyperemic flows. And, indeed, the described relationship between hyperemic MBFs and Δlongitudinal MBF gradient did not necessarily hold anymore for the lower range of the Δlongitudinal MBF gradient, implying an uncoupling of the Δlongitudinal MBF gradient from hyperemic MBFs when high-grade CAD lesions were present. The observed decrease in post-stenotic hyperemic flow, associated with a relative decrease in intracoronary resistance, therefore resulted in a less marked flow gradient than in those coronary vessels without or with less severe focal stenotic lesions but with higher hyperemic flows. The post-stenotic flow gradient, however, is dependent not only on the severity of the epicardial stenosis with a reduction in post-stenotic hyperemic flow, but also on distal artery disease and the extent of branch disease, as previous investigations emphasize (3,9,12).

Myocardial perfusion, MFR, and epicardial stenosis. The visual or semiquantitative assessment of

Table 4. Diagnostic Accuracy of PET/CT-Determined MFR and ΔLongitudinal MBF Gradient in the Detection of Epicardial Stenosis ≥50% in CAD Patients

	MFR	ΔLongitudinal MBF Gradient	Combined
Sensitivity	71 (40/56)	88 (49/56)	100 (56/56)
Specificity	63 (10/16)	81 (13/16)	75 (12/16)
PPV	87 (40/46)	94 (49/52)	93 (56/60)
NPV	38 (10/26)	65 (13/20)	100 (12/12)
Diagnostic Accuracy	70 (50/72)	86 (62/72)	94 (68/72)

Values are % (n/N) on a vessel-based analysis.
Abbreviations as in Tables 1 and 2.

stress-induced regional myocardial perfusion defects on single-photon emission computed tomography or PET images commonly signifies the "culprit lesion" in multivessel CAD, but the hemodynamic significance of the remaining epicardial lesions of less or intermediate severity may be missed (1). In principle, this limitation may be overcome by absolute MBF quantification with PET, or nowadays with PET/CT imaging. The ability of PET imaging to concurrently assess regional resting and hyperemic MBFs with the calculation of the MFR principally affords the identification of the hemodynamic significance of each epicardial lesion in coronary multivessel disease (4,7,15).

There are several clinical investigations (2,16–18) that have strived to identify the optimal threshold values of hyperemic MBFs or MFR to identify epicardial lesions. These threshold values of hyperemic MBF or MFR, however, are dependent on the PET methodology, the radiotracer applied for the assessment of MBF, and the definition of morphologically-significant epicardial lesions (7,15). For example, in a recent investigation (16), the diagnostic value of hyperemic MBF, MFR, and the relative radiotracer content (mCi/ml) for detecting coronary stenosis ≥70% among patients with suspected or known CAD was investigated with ^{13}N-ammonia PET. A cut-point analysis for sensitivity, specificity, and accuracy demonstrated the optimal MBF criteria for CAD when a hyperemic MBF threshold value of <1.85 ml/g/min and the best relative tracer content as <70% maximum was applied. In addition, an abnormal MFR was defined as <2.0. Applying these ^{13}N-ammonia PET perfusion and flow parameters, the ROC analysis in the evaluation of the diagnostic accuracy of CAD lesions demonstrated the highest value of 0.90 for adenosine-stimulated absolute hyperemic MBF, 0.86 for MFR, and 0.69 for ^{13}N-ammonia relative uptake. In a more recently performed investigation, Fiechter et al. (2) also used a pre-defined MFR threshold of ≤2.0 for predicting CAD lesions with a luminal narrowing ≥50%. Employing this pre-defined threshold of MFR resulted in a sensitivity, specificity, and diagnostic accuracy of 96%, 80%, and 92% for detecting epicardial lesions. In the current study, we used an ROC-defined threshold of ≤1.40 for the MFR for the detection of ≥50% diameter stenosis in patients with predominantly multivessel CAD. Operating this MFR threshold of 1.40 resulted in a sensitivity, specificity, and diagnostic accuracy of 71%, 63%, and 70%, respectively, in the identification of CAD lesions. The relatively low sensitivity and, in particular, specificity may be surprising as compared with a recent investigation (2), but most likely it is related to the lower MFR threshold of 1.40 for CAD identification and the presence of more advanced stages of CAD commonly associated with more pronounced microvascular dysfunction (7). The latter consideration may agree with the observation that hyperemic MBFs in the myocardial territories without stress-induced perfusion defects but with or without stenosis of ≥50% were comparable. Further support also comes from recent observations (1) in a cohort of 120 consecutive patients referred to a dipyridamole ^{82}rubidum PET for the detection of myocardial ischemia. As it was observed, among 25 patients with severe 3-vessel CAD, MFR was globally diminished in 22 (88%) of these patients

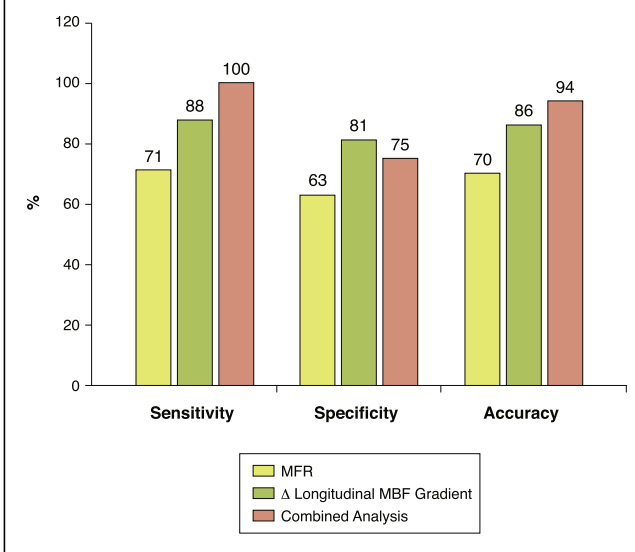

Figure 3. Sensitivity, Specificity, and Diagnostic Accuracy of MFR, ΔLongitudinal MBF Gradient, or Both in the Detection of Epicardial Stenosis ≥50%

Schematic representation of the sensitivity, specificity, and diagnostic accuracy of positron emission tomography–measured MBF hyperemic flow parameters in the detection of epicardial stenosis. Abbreviations as in Figure 1.

when a MFR threshold of <2.0 was applied. When applying another radiotracer, such as ^{15}O-water, a threshold of pharmacologically-induced hyperemic MBFs of <2.5 ml/g/min was demonstrated to be most accurate in the identification of epicardial lesions of >50% diameter stenosis (17). In a more extended investigation by Kajander et al. (18), 104 patients with moderate (30% to 70%) pre-test likelihood of CAD underwent ^{15}O-water PET perfusion imaging. Applying a hyperemic MBF threshold <2.5 ml/g/min for the detection of CAD resulted in a sensitivity, specificity, and diagnostic accuracy of 95%, 91%, and 92%, respectively, which are comparable to those values as determined with ^{13}N-ammonia PET using a MFR threshold of <2.0 for CAD identification (2).

Longitudinal myocardial flow gradient. In the current study, using invasive quantitative coronary angiography as reference, we performed a ROC analysis to define the optimal threshold for the identification of epicardial stenosis ≥50% by a Δlongitudinal MBF gradient and corresponding MFR. Relying exclusively on the Δlongitudinal MBF gradient and MFR, the ROC analysis defined thresholds of ≤0.25 ml/g/min and ≤1.40, respectively, to identify CAD lesions. Applying these thresholds in the current study, the sensitivity and specificity of the Δlongitudinal MBF gradient was significantly higher as compared with the MFR (88% vs. 71% and 81% vs. 63%, respectively). This also manifested in a higher diagnostic accuracy to signify CAD lesions, with 86% for the Δlongitudinal MBF gradient as compared with 70% when the MFR was applied. In addition, when combining both quantitative flow parameters as determined with PET, considering the presence or absence of epicardial stenosis ≥50% to be significant when identified by 1 of the 2 flow parameters, the diagnostic accuracy was significantly increased to 94%. In this direction, the sensitivity increased to 100%, and the specificity turned intermediate to 75%. Overall, the combined evaluation of both flow parameters yielded the highest diagnostic accuracy in the evaluation of epicardial lesions compared with the separate analysis of Δlongitudinal MBF gradient or MFR. Combining both flow parameters, therefore, could evolve as a preferred approach in the evaluation of epicardial lesions in multivessel disease, but further clinical validation is needed.

Study limitations. In view of the relatively small sample size of a selected study population with suspected (n = 20) and known (n = 4) CAD, the current findings may be appreciated more as a "proof principle" study. Conversely, these initial observations may provide an important framework to initiate larger clinical trials to draw more definite conclusions. Further, MBFs in the mid and mid-distal LV segments were measured and, thus, the longitudinal MBF gradient was determined over a relatively short longitudinal distance aiming to circumvent confounding count variability in the basal segments and partial volume effects in the apical segment on MBF measurements. This, again, may have led to some underestimation of the longitudinal MBF gradient during hyperemic flows. With the advent of PET/magnetic resonance imaging (19), an optimal partial volume correction also in the apical segments appears to be feasible, which should lead to a more refined assessment of the longitudinal MBF gradient. Notably, combining 3-dimensional fusion of CT-determined coronary morphology and myocardial flow on a voxel basis (18) would also afford reliable measurement of a longitudinal flow gradient during pharmacologic vasodilation not only in the post-stenotic myocardial region, but also before and after a given CAD lesion. The latter diagnostic approach could hold promise for the development of a noninvasive fractional flow reserve.

CONCLUSIONS

The observed correlation between focal epicardial stenosis severity and a post-stenotic Δlongitudinal MBF gradient further supports the validity and value of the longitudinal MBF gradient as a noninvasive index of the severity of epicardial stenosis. Furthermore, the combined evaluation of a post-stenotic longitudinal ΔMBF gradient and corresponding MFR may evolve as a new promising analytic approach to further optimize the identification of CAD lesions in multivessel disease, but further clinical investigation is needed.

Acknowledgments

The authors thank Christina Laemmli, Stephan Dewarrat, and Claude Ponsolle for assisting in the PET studies, and the cyclotron staff for ^{13}N-ammonia production.

Reprint requests and correspondence: Dr. Thomas H. Schindler, Division of Nuclear Medicine, Cardiovascular Nuclear Medicine, Department of Radiology and Radiological Science SOM, Johns Hopkins University, JHOC 3225, 601 North Caroline Street, Baltimore, Maryland 21287. *E-mail:* Thomas.h.schindler@gmail.com.

REFERENCES

1. Ziadi MC, Dekemp RA, Williams K, et al. Does quantification of myocardial flow reserve using rubidium-82 positron emission tomography facilitate detection of multivessel coronary artery disease? J Nucl Cardiol 2012;19:670–80.
2. Fiechter M, Ghadri JR, Gebhard C, et al. Diagnostic value of 13N-ammonia myocardial perfusion PET: added value of myocardial flow reserve. J Nucl Med 2012;53:1230–4.
3. Gould KL, Johnson NP, Bateman TM, et al. Anatomic versus physiologic assessment of coronary artery disease: guiding management decisions using positron-emission tomography as a physiologic tool. J Am Coll Cardiol 2013;62:1639–53.
4. Sdringola S, Johnson NP, Narula J, Gould KL. Serial quantitative assessment of absolute coronary flow and flow reserve with CAD progression to events. J Am Coll Cardiol Img 2013;6:735–8.
5. Ziadi MC, Dekemp RA, Williams KA, et al. Impaired myocardial flow reserve on rubidium-82 positron emission tomography imaging predicts adverse outcomes in patients assessed for myocardial ischemia. J Am Coll Cardiol 2011;58:740–8.
6. Herzog BA, Husmann L, Valenta I, et al. Long-term prognostic value of 13N-ammonia myocardial perfusion positron emission tomography added value of coronary flow reserve. J Am Coll Cardiol 2009;54:150–6.
7. Schindler TH, Schelbert HR, Quercioli A, Dilsizian V. Cardiac PET imaging for the detection and monitoring of coronary artery disease and microvascular health. J Am Coll Cardiol Img 2010;3:623–40.
8. Naya M, Murthy VL, Foster CR, et al. Prognostic interplay of coronary artery calcification and underlying vascular dysfunction in patients with suspected coronary artery disease. J Am Coll Cardiol 2013;61:2098–106.
9. Gould KL, Nakagawa Y, Nakagawa K, et al. Frequency and clinical implications of fluid dynamically significant diffuse coronary artery disease manifest as graded, longitudinal, base-to-apex myocardial perfusion abnormalities by noninvasive positron emission tomography. Circulation 2000;101:1931–9.
10. Hernandez-Pampaloni M, Keng FY, Kudo T, Sayre JS, Schelbert HR. Abnormal longitudinal, base-to-apex myocardial perfusion gradient by quantitative blood flow measurements in patients with coronary risk factors. Circulation 2001;104:527–32.
11. Sdringola S, Patel D, Gould KL. High prevalence of myocardial perfusion abnormalities on positron emission tomography in asymptomatic persons with a parent or sibling with coronary artery disease. Circulation 2001;103:496–501.
12. Valenta I, Quercioli A, Vincenti G, et al. Structural epicardial disease and microvascular function are determinants of an abnormal longitudinal myocardial blood flow difference in cardiovascular risk individuals as determined with PET/CT. J Nucl Cardiol 2010;17:1023–33.
13. De Bruyne B, Hersbach F, Pijls NH, et al. Abnormal epicardial coronary resistance in patients with diffuse atherosclerosis but "Normal" coronary angiography. Circulation 2001;104:2401–6.
14. Scanlon PJ, Faxon DP, Audet AM, et al. ACC/AHA guidelines for coronary angiography: a report of the American College of Cardiology/American Heart Association Task Force on Practice Guidelines (Committee on Coronary Angiography). J Am Coll Cardiol 1999;33:1756–824.
15. Johnson NP, Kirkeeide RL, Gould KL. Is discordance of coronary flow reserve and fractional flow reserve due to methodology or clinically relevant coronary pathophysiology? J Am Coll Cardiol Img 2012;5:193–202.
16. Hajjiri MM, Leavitt MB, Zheng H, et al. Comparison of positron emission tomography measurement of adenosine-stimulated absolute myocardial blood flow versus relative myocardial tracer content for physiological assessment of coronary artery stenosis severity and location. J Am Coll Cardiol Img 2009;2:751–8.
17. Nesterov SV, Han C, Mäki M, et al. Myocardial perfusion quantitation with 15O-labelled water PET: high reproducibility of the new cardiac analysis software (Carimas). Eur J Nucl Med Mol Imaging 2009;36:1594–602.
18. Kajander SA, Joutsiniemi E, Saraste M, et al. Clinical value of absolute quantification of myocardial perfusion with (15)O-water in coronary artery disease. Circ Cardiovasc Imaging 2011;4:678–84.
19. Nensa F, Poeppel TD, Beiderwellen K, et al. Hybrid PET/MR imaging of the heart: feasibility and initial results. Radiology 2013;268:366–77.

Key Words: blood flow ■ CAD ■ circulation ■ coronary stenosis ■ flow gradient ■ MFR ■ microvascular function ■ myocardial perfusion ■ PET.